AFS Transactions 2007 © American Foundry Society, Schaumburg, IL USA

The Effect of Porosity on the Fatigue Life of 8630 Cast Steel

P.T. Deegan, R.I. Stephens, R.A. Hardin, C. Beckermann
Department of Mechanical and Industrial Engineering, University of Iowa, Iowa City, Iowa

ABSTRACT

Fatigue testing of cast 8630 steel with porosity levels ranging from microscopic to macroscopic levels was performed. Low-cycle and high-cycle fatigue tests with an R-ratio of -1 were conducted using strain- and stress-control, respectively. Fractography and microscopy were used to relate fatigue resistance to porosity. Fatigue resistance was directly related to the material soundness, type, size and quantity of porosity. Comparisons showed keel block material gave the best fatigue resistance, followed closely by steel cast in a truncated cone shape having microporosity and then by steel cast as straight cylinders having macroscopic centerline shrinkage porosity. Fatigue resistance decreased as porosity size and quantity increased. The fatigue limit at 2 x10^6 cycles ranged from 293 MPa to less than 40 MPa for sound to centerline shrinkage porosity, respectively.

INTRODUCTION

Porosity in castings seriously affects the design of a component. Pores within a material act as local stress risers and can lead to the nucleation of cracks that may eventually lead to fracture. To compensate for this, designs for castings are often overbuilt and in turn raise manufacturing costs and part weight. The current research has been directed to determining how pores develop in castings, and their effect on the fatigue life of the material. It has been found that a strong temperature gradient reduces the amount of porosity that forms, but complex geometries can often produce porosity, even in the presence of risers or chills. By implementing methods to try and control the temperature gradient, the cost of casting rises due to more complex molds and more post processing such as machining. These costs can be managed by predicting the presence and effect of porosity in the critical areas of a component, especially in cyclically loaded regions. Casting process simulations were used to design as-cast steel material with varying amounts of porosity that was machined into test specimens. Specimens were mechanically tested to investigate the effect of porosity on fatigue life. By incorporating results from two previous studies with results from the current research, a more comprehensive view of the detrimental effect of porosity on axially loaded 8630 cast steel has been determined.

Research on the effect of porosity on fatigue life has been conducted on different materials. Cast aluminum has been used in many studies, including a study by Wang et al.[1] using axially loaded specimens. Specimens with porosity were compared to sound material and specimens containing other factors such as oxide films, eutectic particles, and slip bands. It was found that specimens failing from oxide films had 4-5 times longer life, and the sound specimens had a 25 times longer life than porous specimens. In the same study the final fracture surface indicated a higher concentration of pores than was observed on metallographic measurements. This showed that final fracture seeks out the weakest path that links the largest amount of pores through microcracks. It was concluded that porosity was the most detrimental discontinuity to fatigue performance. Buffiere et al.[2] tested cast aluminum with varying amounts of induced porosity. The specimens were axially loaded, and the results indicated that castings with as little as 1% porosity volume fraction had a 50% reduction in fatigue life, and a 20% reduction in fatigue limit. The study concluded that the pore size distribution, and number of pores are major factors affecting fatigue life. Their method for inducing porosity not only controlled the volume fraction of pores, but also increased the average pore size as the volume fraction increased.

Fractography has revealed that pores at, or near, the surface were almost always sites where the fatigue crack initiated. Maino and Wallace[3] specifically studied surface porosity in cast aluminum. Using fully reversed bending, surface cavities were shown to have a serious effect on the fatigue life. The fatigue strength was decreased 16-32% for various sized cavities at 10^5 cycles, and decreased further at 10^6 cycles. Fractures were generally found to initiate at the largest surface pore. Cast stainless steel was tested in rotating bending by Kohno and Makioka[4] to study the effect of pore size using centerline shrinkage porosity. It was found that pores less than 10% of the diameter of test section had no effect on the fatigue life as long as the pore was on the centerline. However, Chijiwa et al.[5] found if the shrinkage cavity was off the centerline or larger than 10% of the test section diameter the fatigue life decreased along with the fatigue limit.

Here the results of two previous studies are presented with the results of current research to develop a better understanding of the difference in fatigue lives between varying levels of porosity and sound castings. The first study was conducted for the

Steel Founder's Society of America (SFSA)[6]. This study tested 8630 cast steel for fatigue and cyclic properties along with other steels. The specimens used for testing were machined from keel blocks that are generally considered a reliable method for obtaining sound castings. Fully reversed testing was conducted on specimens that conformed to ASTM Standard E606 for standard practice in strain control fatigue testing, and these results are used for the comparison of sound material properties. The second study was also conducted for the SFSA by Sigl et al.[7] and results were published in 2003. The results of the study provide fatigue lives of two levels of porosity for 8630 cast steel. The specimens were machined to the same specification and size as the 1983 SFSA study. The first level of porosity was a microporous casting that was cast in the shape of a cylinder with a tapered center. Radiography of these specimens showed a sound specimen. However, through the use of microscopy, the specimen test sections revealed micropores in the material that are not indicated by x-rays. Sigl used this cast shape to machine specimens for both monotonic and fatigue testing. The second level of porosity involved macroporous material. The shape of the casting was a cylinder with a disc at the center. The purpose of this shape was to induce porosity at the disc, where a specimen was machined with the predicted porosity in the reduced test section. Fatigue testing was conducted on these specimens that yielded much lower fatigue lives than the microporous specimens and greatly reduced the effective modulus of elasticity.

TEST MATERIAL AND METHODS

TEST MATERIAL/SPECIMENS

Specimen blanks for the current research were cast using AISI 8630 steel. Two cylindrical geometries were designed for the as-cast specimen blanks. Figure 1 shows the dimensions of the specimen and the two as-cast blanks; a cylinder and a truncated cone. The mold fills from the gating into the bottom to each specimen blank, each with a diameter of 25 mm. The specimens were designed to have either porosity detectable by radiograph (for the straight cylinder) or without detectable porosity (for the truncated cone). Each as-cast blank had a 52 mm diameter by 72 mm tall vented riser. The truncated cone shape was used to create a strong temperature gradient to minimize the formation of porosity. The height of the truncated cone blank was 158 mm to the riser, and had a diameter of 52 mm at the top where the riser began. The straight cylinder blanks had a height of 158 mm and a diameter of 25 mm. The straight cylinder was designed to produce centerline porosity.

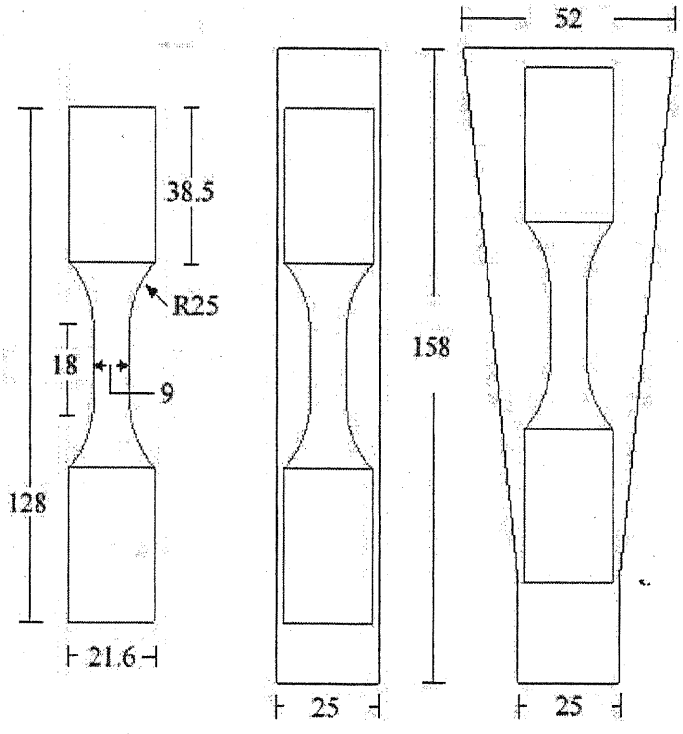

Figure 1 Dimensions in mm of test specimens and as-cast cylinders and truncated cones

Ten molds were formed from a no-bake chemical sand mold with Pepset binder. The castings were produced and heat treated at Southern Cast Products in Meridian, Mississippi. After casting, the blanks were normalized at 900°C, then austenized at 885°C, water quenched, and tempered at 510°C for 1.5 hours. Two separate truncated cone specimens were used to measure the machined specimen hardness. Preparation and hardness testing of the specimen cross section was done in accordance with ASTM standard E18[8]. Five separate tests were taken across the face of each specimen and averaged 36 on the Rockwell C scale. This method tested the internal hardness and not the surface of the specimen. The final composition by weight was

1.06% Mn, 0.82% Cr, 0.57% Ni, 0.38% Si, 0.31% Mo, 0.28% C, 0.010% P, and 0.007% S. The quantities found are close to the standards set forth by the Steel Casting Handbook[9] for wrought AISI 8630 steel, and similar to the material used in the SFSA and Sigl studies.

The specimen dimensions were based on ASTM standard E606[10] that sets standards for strain controlled testing. These standards are also compatible for load controlled testing as well. In previous testing conducted by Sigl[7], the ratio of porosity to cross sectional testing area was large (up to 50%) and testing produced results that were difficult to compare to the other levels of porosity. In order to reduce this effect, a larger specimen was deemed necessary for this research. The new diameter for the test section was set at 9 mm, while the previous testing used a diameter of 5 mm, resulting in a cross sectional area gain of 223%. The test section after machining was polished to a surface roughness of less than 0.2 microns with the direction of the final scratches going longitudinally.

RADIOGRAPHY AND TESTING PROCEDURES

For inspection of macroporosity the machined specimens were taken to Alloyweld Inspection Company, Inc. of Bensenville, Illinois to conduct radiography. There is a limit to the resolution which is determined by the section thickness, and generally pores cannot be resolved that are less than 2% of the section thickness. Based on the thickest part of the test section of 9 mm the smallest pore resolved would be around 200 microns, and anything smaller would be considered microporosity. Through inspection of the radiographs, larger diameter porosity or a high density of porosity could be viewed in the specimens as dark regions. Figure 2 shows representative specimen test section radiographs from four truncated cone blanks with the gage length and location of fracture region indicated. It can be seen that there is no evidence of macroporosity in any of the specimen areas. The straight cylinder blank specimens showed macroporosity throughout much of the test section as shown for four specimens in Figure 3 where the gage length and fracture region are indicated for each specimen.

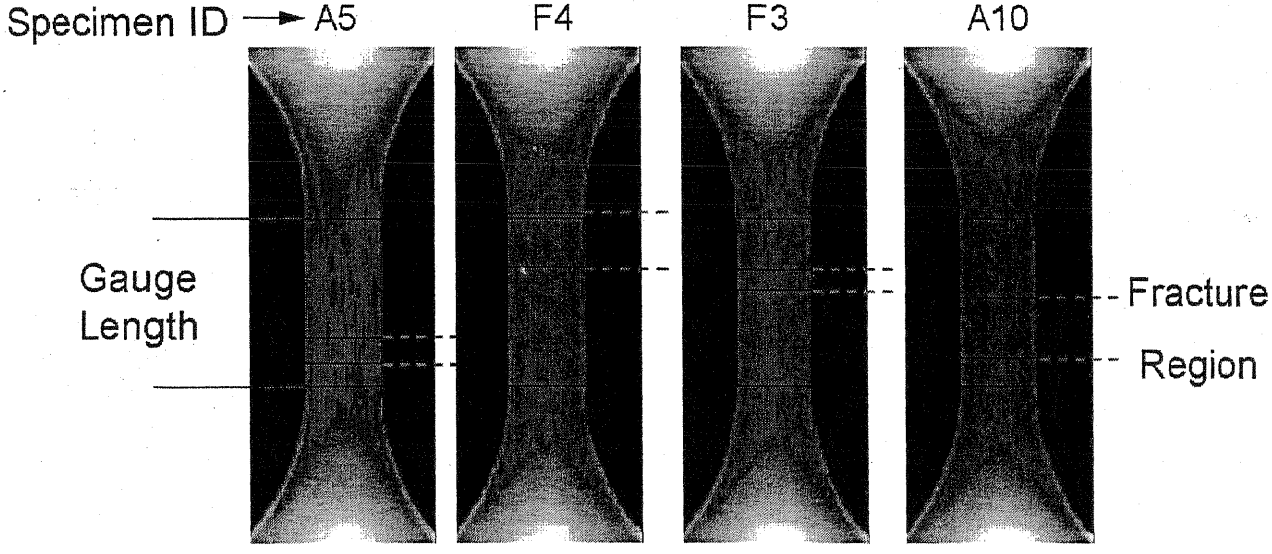

Figure 2 Representative radiographs of truncated cone specimens

Tests were performed to determine the tensile properties of yield and ultimate strengths (S_{yt}, S_{ut}), percent reduction of area (%RA), and the modulus of elasticity (E). Fatigue testing was conducted using a closed loop servo-hydraulic test system and specimens were gripped using hydraulic V-notched wedge grips with inserts designed for diameters 17-22.9 mm. Data were collected with a 100 kN load cell and a 12.5 mm extensometer. Fatigue tests were conducted using a computer controlled fatigue testing application. All tests were conducted in a fully reversed, R=-1 condition. R in strain control is defined by Equation (1) where ε_{min} and ε_{max} are the limits of the strain range. Under load control R is defined by Equation (2) and σ_{min} and σ_{max} are the limits of the stress range based on the nominal cross sectional area of the specimen test section.

$$R = \frac{\varepsilon_{min}}{\varepsilon_{max}} \qquad \text{Equation 1}$$

$$R = \frac{\sigma_{min}}{\sigma_{max}} \qquad \text{Equation 2}$$

Under low cycle fatigue (LCF) conditions, where the specimen underwent plastic deformation, tests were conducted under constant strain amplitude with a triangular wave form and frequencies less than one Hertz. Tests were terminated once the specimen fractured or a drop in load of more than 75% occurred. If the strain amplitude was determined to be predominantly

elastic, then testing was accomplished using load control. The loads specified were calculated from stresses based on the nominal cross sectional area of the specimen. Since the strain levels were lower under elastic deformation, tests were run using a sinusoidal wave form using the high cycle fatigue (HCF) setting in the fatigue testing software. Cyclic frequencies were increased to 3-15 Hz, and the test termination occurred when the specimen fractured.

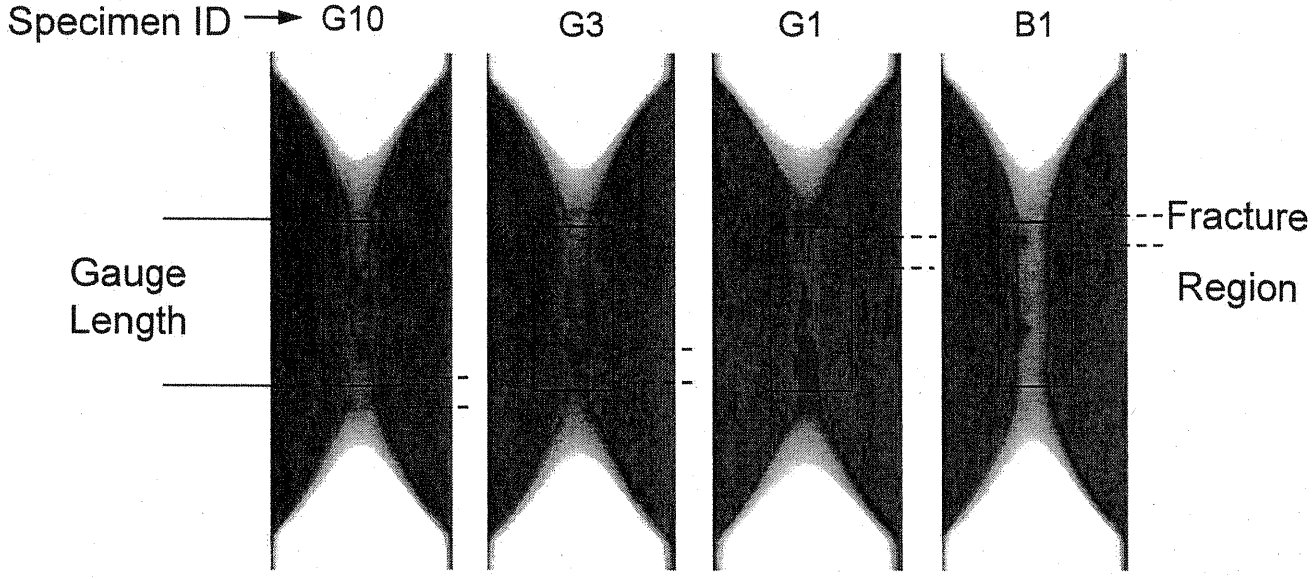

Figure 3 Representative radiographs of straight cylinder specimens

Twelve truncated cone specimens were used to construct strain-life (ε-N) and stress-life (S-N) fatigue curves. Starting at 0.01 strain amplitude, the testing decreased in amplitude using LCF. All tests were conducted at 0.25Hz while the amplitude was decreased to 0.008, 0.006, 0.005, 0.004, and finally 0.0035 for different specimens. At a strain amplitude of 0.0035 the deformation was almost entirely elastic. Additionally one specimen was tested in strain control using an incremental method to determine cyclic stress-strain behavior. This method cycles the specimen at a specific strain amplitude until a steady load is achieved, then the amplitude is increased. The data obtained from this single test were used to compliment the cyclic stress-strain properties gained from the companion method. The companion method uses the multiple fatigue specimens where each specimen is tested at single stress/strain amplitude until failure. Then representative stress and strain data were used from each specimen to determine the cyclic stress-strain properties.

The truncated cone testing was then switched to HCF using load control so that the frequency could be increased. The same decrease in strain amplitude (ε_a) defined in Equation (3) started in LCF testing was continued in HCF testing. This was accomplished by calculating the alternating stress (σ_a) based on the nominal cross sectional area divided by the average modulus of elasticity (E) from the monotonic tests.

$$\varepsilon_a = \frac{\sigma_a}{E} \qquad \text{Equation 3}$$

The first HCF specimen was started at the amplitude of 587 MPa that corresponds to a calculated strain amplitude of 0.003. The predetermined run-out value of $2x10^6$ cycles was achieved at a stress amplitude of 197 MPa that corresponds to a calculated strain amplitude of 0.001. The stress amplitude was stepped down from 587 to 197 MPa at calculated intervals. The frequency was also increased from the initial rate of 3Hz with the final specimen running at 15Hz.
Ten specimens were machined from the straight cylinder blanks and were tested in similar fashion to the HCF truncated cone specimens. The main interest was to investigate the long life fatigue behavior of these specimens, and it was predicted that the lives would be shorter than the truncated cone specimens due to porosity. For comparison to the truncated cone specimens, three lower stress levels of 587, 394, and 196 MPa were used to begin testing. These corresponded to the truncated cone specimen stress amplitudes where the lowest level was the truncated cone specimen run-out level. Run-out did not occur at a stress level of 196 MPa, so testing continued at two lower stress levels of 147 and 127 MPa where the lower level achieved the run-out criterion of $2x10^6$ cycles. Two specimens were tested at each level for duplication purposes.

EXPERIMENTAL RESULTS

MONOTONIC PROPERTIES

Monotonic properties were obtained by using two truncated cone blank specimens. Results are shown in Table 1 along with comparison to the benchmark values found in 1983[6] and the work done in 2003 by Sigl et al[7]. Figure 4 shows the stress versus strain for the two monotonic specimens. The average yield (0.2% offset) and ultimate strengths in tension (S_{yt}, S_{ut}) were found to be 1124 MPa and 1183 MPa respectively for the truncated cones. The S_{ut} average values for all data sets were quite similar, however, S_{yt} for the current data set was slightly higher than the SFSA data as shown in Table 1. For each test, both truncated cone specimens showed necking before failure with considerable plastic deformation that is reflected in the average percent reduction of area (%RA) of 13. The %RA found from the 1983 keel block specimens is greater than the new data obtained; this difference could be accounted for by the yield strength difference. By taking a linear regression of the elastic part of the monotonic test curve the modulus of elasticity (E) was found to be an average of 196 GPa which was close to the previous research values.

Table 1 Average Properties from Monotonic Tests

Property	Truncated Cone (2006)	Sigl Microporous (2003)	SFSA Keel Block (1983)
S_u (MPa)	1 183	1 125	1 144
S_y (MPa)	1 124	1 088	985
E (GPa)	196	197	207
%RA	13	7	29

TRUNCATED CONE CYCLIC AND FATIGUE PROPERTIES

Twelve specimens machined from the truncated cone blanks were used to develop the fatigue properties. The results can be found in Table 2 with comparison to the 1983 results[6] and the Sigl 2003 microporous specimens[7]. The fatigue strength (S_f) at $2x10^6$ cycles of 208 MPa is lower than the 1983 property of 293 MPa, but higher than the Sigl value of 126 MPa, both found at $5x10^6$ cycles. Using $2x10^6$ or $5x10^6$ cycles does not affect the values of S_f for these data. Figure 4 shows the cyclic stress-strain behavior directly compared with the two monotonic curves from truncated cone specimens. The cyclic stress-strain

Table 2 Cyclic and Fatigue Properties

Property	Truncated Cone (2006)	Sigl Microporous (2003)	SFSA Keel Block (1983)
S_f (MPa)	208	126	293
S_f/S_u	0.18	0.11	0.26
K′ (MPa)	1 842*	2 550	1 502 / 2 267#
n′	0.122*	0.167	0.122 / 0.195#
S_y' (MPa)	840	894	682 / 661#
b	-0.185	-0.176	-0.121
c	-0.801	-0.908	-0.693
σ_f'(MPa)	3 214	2 390	1 936
ε_f'	0.23	0.11	0.42

determined from companion and incremental step methods, respectively.

* integrated using companion and incremental step methods.

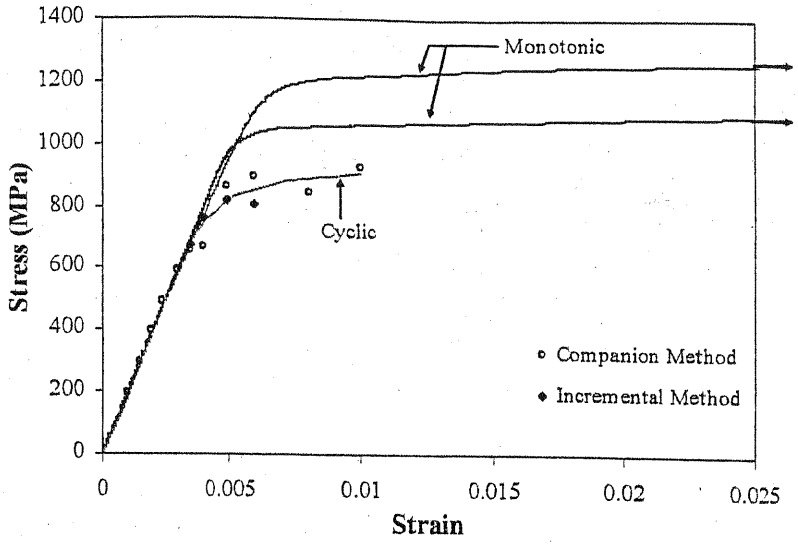

Figure 4 - Monotonic and cyclic stress-strain curves for truncated cone specimens.

curve was developed using data from both the companion and incremental methods. For tests conducted in low cycle fatigue the strain amplitude was held constant for each specimen. This allowed the stress to vary for cyclic softening or hardening, or as cracking developed and the specimen fractured. A stress was needed from the tests so a single cycle was chosen as representative. The ASTM standard E606[10] suggests using an approximate half-life for determining stress in strain control testing; however, in this case at the approximate half-life point the specimen might not show a valid representation of the behavior. In order to find a steady state behavior for a specimen a variation of the standard was used. This was accomplished using the relationship of stress amplitude to normalized life which is shown in Figure 5. During the first cycles the specimen cyclic softened or hardened, while during the final cycles the stress dropped significantly which indicates macro cracking before failure. A quasi-steady state appears in the initial third of the fatigue life before cracking develops, but the stress for higher strain amplitudes never has a steady load applied for a significant part of the life. The approximate halfway point on the quasi-steady state was chosen for representative stress data. Figure 6 shows the representative stress-strain hysteresis loops from the four greatest strain amplitude specimens used in the companion method. To augment these cyclic stress-strain results, the incremental test results have been incorporated with the companion strain control specimens. The hysteresis loops of the three greatest strain amplitude tests for the incremental method are shown in Figure 7.

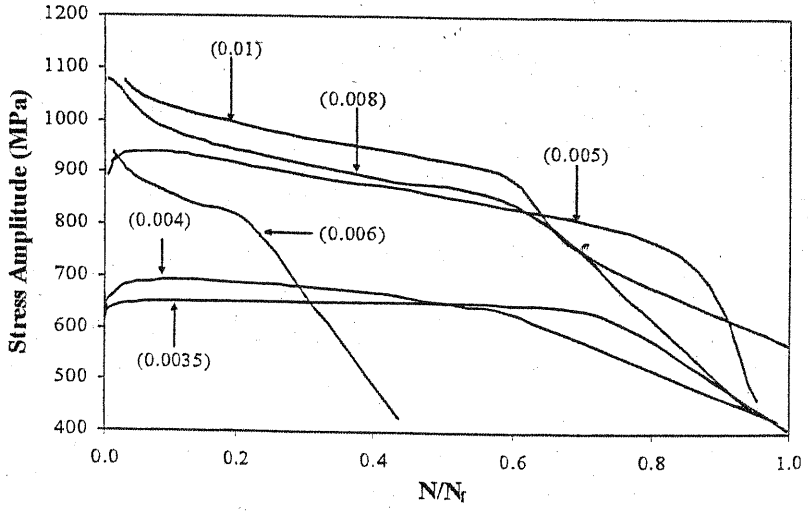

Figure 5 Stress amplitude vs. normalized applied cycles for LCF truncated cone specimens.

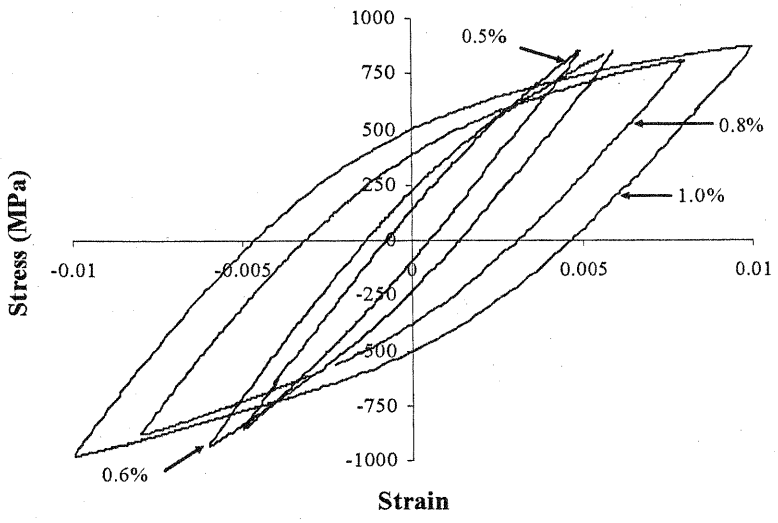

Figure 6 Stress-strain hysteresis loops for LCF testing (Companion Method).

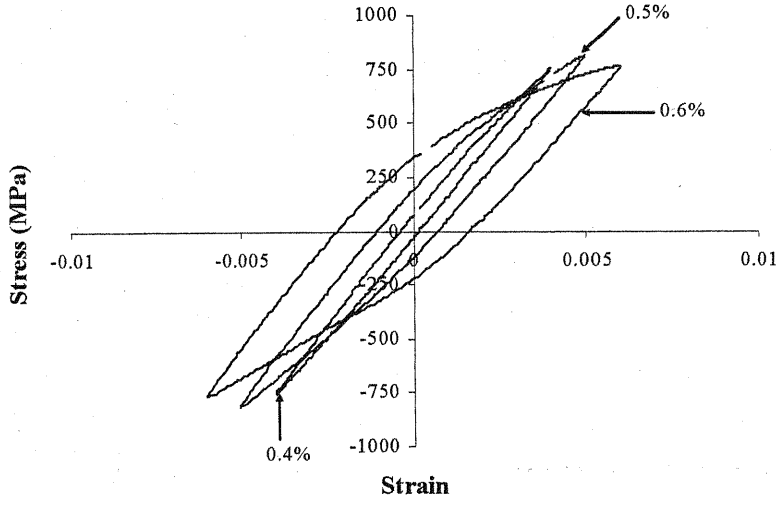

Figure 7 Stress-strain hysteresis loops for LCF testing (Incremental Method).

For each specimen a hysteresis cycle, as described previously, of the total strain can be broken into two components: the plastic and elastic components. The amount of total strain induced in these tests was below 2%. The values can be assumed to be true stress and strain (σ, ε) because the difference is negligible between the engineering values and the true values based on the instantaneous cross-sectional area. By plotting the stress amplitude versus plastic strain amplitude of the companion and incremental specimens, a power law best fit line regression was used to determine the cyclic strength coefficient (K′) and strain hardening exponent (n′). This can be defined in Equation (4):

$$\sigma_a = K'\left(\frac{\Delta\varepsilon_p}{2}\right)^{n'} \qquad \text{Equation 4}$$

Using total elastic and plastic strain amplitudes ε-N curves were constructed using the twelve fatigue specimens. Equation (5) uses the elastic strain amplitude ($\Delta\varepsilon_e/2$) with the monotonic modulus of elasticity (E) versus the reversals to failure ($2N_f$) to determine the fatigue strength coefficient (σ_f'), and the fatigue strength exponent (b) from least squares curve fitting of the test data.

$$\frac{\Delta\varepsilon_e}{2} = \frac{\sigma_f'}{E}(2N_f)^b \qquad \text{Equation 5}$$

The fatigue ductility coefficient (ε_f') and fatigue ductility exponent (c) are found in the same manner using the plastic strain amplitude ($\Delta\varepsilon_p/2$) in Equation (6):

$$\frac{\Delta\varepsilon_p}{2} = \varepsilon_f'(2N_f)^c \qquad \text{Equation 6}$$

The combination of these two curves is used to construct the total strain-life behavior of the truncated cone specimens as shown in Figure 8. Power law line regression was applied using stress amplitude (S_a) versus cycles to failure (N_f) to create a stress-life (S-N) curve. This is shown in Figure 9 (solid circular data points) with the trend line characterized as a Basquin equation as given in Equation (7). The alternating stress (σ_a or S_a) is a function of the fatigue strength coefficient (σ_f'), fatigue strength exponent (b), and the reversals to failure (N_f).

$$\sigma_a \text{ or } S_a = \sigma_f'(2N_f)^b \qquad \text{Equation 7}$$

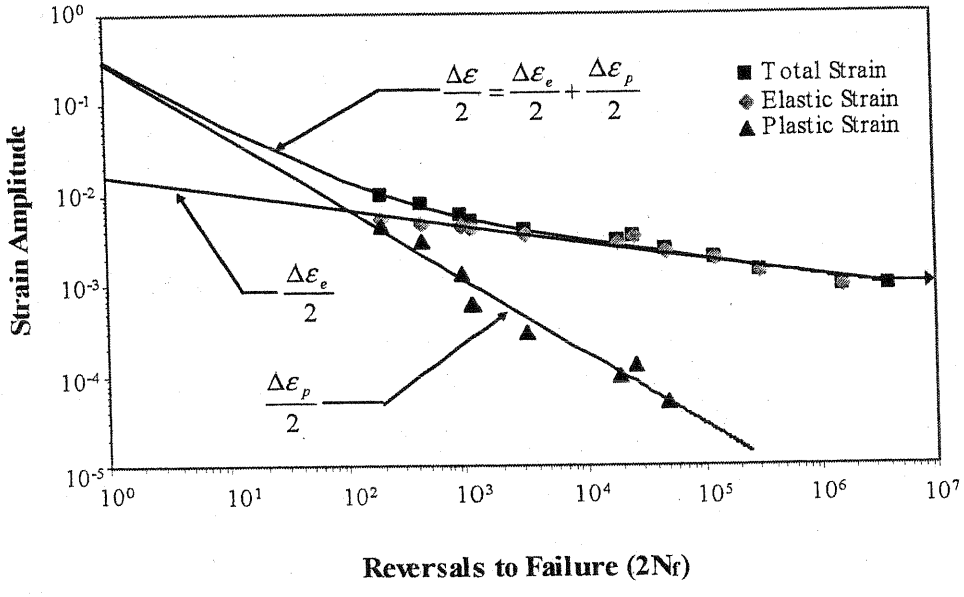

Figure 8 Total, elastic, and plastic strain-life data of truncated cone specimens.

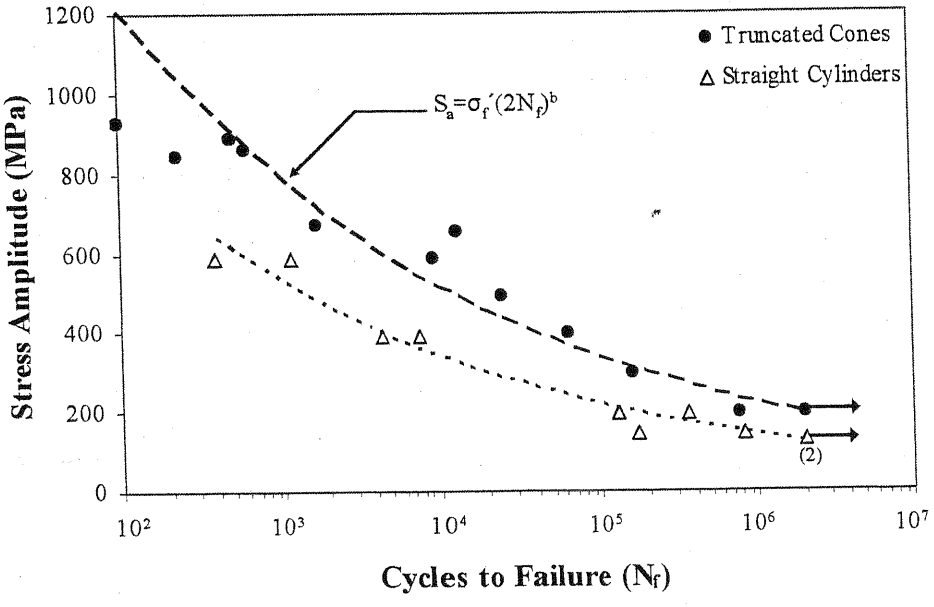

Figure 9 Stress-life results for truncated cone and straight cylinder specimens

STRAIGHT CYLINDER FATIGUE AND PREVIOUS STUDY RESULTS

Specimens machined from straight cylinder blanks were tested in load control at similar R=-1 alternating stress levels to the truncated cone specimens. Using an S-N relationship, the individual specimen results are plotted (open triangle data points) and superimposed on the S-N curve for the truncated cone specimens shown in Figure 9. Two specimens machined from the straight cylinder blank achieved the run-out criterion of $2x10^6$ cycles. Given the fatigue properties from the Sigl study, a Basquin type equation was calculated for the microporous specimens, and a regression line was calculated for the macroporous data. These two S-N relationships based on the Sigl data are shown in Figure 10. A comparison of the Sigl results for both microporous and macroporous specimens to the current research results along with an S-N curve from the SFSA study are shown in Figure 11.

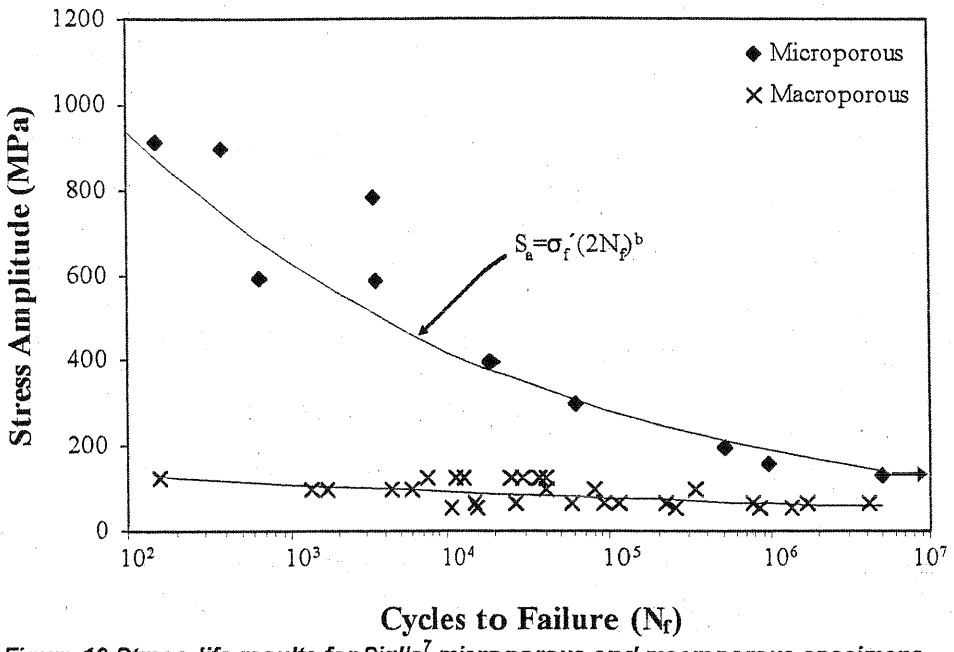

Figure 10 Stress-life results for Sigl's[7] microporous and macroporous specimens.

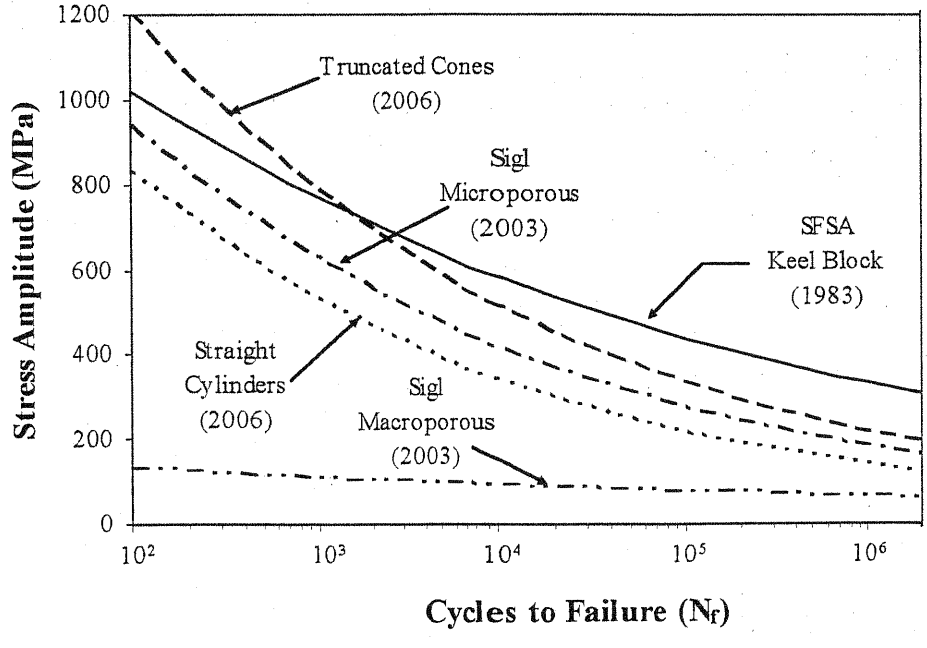

Figure 11 Stress-life results comparison.

The modulus of elasticity (E) was collected and compared from the three different studies. For the current study the strain data from load control testing (HCF) were taken from an approximate half-life cycle of each specimen. A linear regression

was taken assuming totally elastic behavior on the unloading of tension to a zero load, and from this regression an unloading modulus of elasticity was found that represents the particular specimen. The moduli from the Sigl study were also taken from the approximate half-life of the specimen data. The mean and median modulus of elasticity along with the standard deviation for each of the cast blank geometries are given in Table 3.

Table 3 Modulus of Elasticity Statistics

Blank Type	Mean (GPa)	Median (GPa)	Std. Dev. (GPa)
Truncated Cone*	199	204	10.3
Straight Cyclinder	194	197	13.2
Microporous*	201	201	0.8
Macroporous	133	141	21.6

* includes monotonic tests

FRACTOGRAPHY

FRACTOGRAPHY PROCEDURE

After the specimens had been axially tested, several of the fracture surfaces were examined using a scanning electron microscope, including both monotonic and fatigue specimens. As also seen in testing done by Sigl[7], there were two types of fracture morphology; a monotonic type surface, and a more typical fatigue fracture surface. The monotonic type surface was jagged with little evidence of fatigue crack growth (FCG). This type of fracture happened in monotonic specimens as well as specimens that were tested at higher than 0.004 strain amplitude where fatigue lives were less than 1 000 cycles. The other type, a typical fatigue fracture surface, was usually composed of two distinct regions. The first was a macroscopically flat region that showed fatigue facets microscopically, that was typical of a FCG region. Additionally at the edge of the specimen in this region a crack nucleation/initiation site was observed. The second region was the final fracture region that had a shear lip that usually occurred at a 45 ° angle. The angle is indicative of fracture along the plane of the greatest shear stress that is characteristic of a final ductile fracture region. The specimens with the most evidence of fatigue crack growth were found in the HCF specimens. This includes all specimens machined from straight cylinder blanks, and six specimens from the truncated cone blanks.

A Hitachi S-4000 scanning electron microscope (SEM) was employed to conduct fractography. In order to view the specimen fracture surfaces in the SEM, the sections containing the fracture surfaces were cut from the rest of the specimen. The sections were mounted onto an aluminum stage and washed in acetone to remove any contaminants that could affect the image. Images were taken at 20x and 1500x inline with the applied axial load.

All the specimen fracture surfaces were examined by eye to choose a representative fracture from the two different casting geometries. The fracture surfaces shown in the following figures focus on the longer life specimens that were conducted under stress control. Additionally, representative fractography for similar specimens from the Sigl study are also incorporated for direct comparison. Unfortunately no constant amplitude fractography was available from the SFSA study.

TRUNCATED CONE SPECIMEN FRACTOGRAPHY RESULTS

The truncated cone specimens exhibited two types of fatigue fracture. The first type of fracture looked similar to a monotonic fracture with mostly ductile deformation and little evidence of FCG. These fractures were seen in low fatigue life, high strain amplitude LCF specimens. The other type of fracture was a typical fatigue fracture as seen in Figure 12. The typical fatigue fracture contained two regions that are indicated by a white line in the figure. The FCG region is seen to the left of the dividing line, and the right side is the final fracture region. The FCG region was generally flat and under higher magnifications showed fatigue facets as seen in the left side of Figure 13. The final fracture region was usually angled at 45° and contained microscopic ductile dimples shown in right side of Figure 13. Ductile dimples are a sign of a high energy ductile fracture. The dashed line box in Figure 12 indicates the region of the close up fractograph in Figure 12 and shows dendrite formation where the fatigue crack nucleated. Fracture surfaces of all the truncated cone specimens examined had some evidence of dendrite formation. Dendrites can be the result of the liquid metal crystallizing as a free surface. The presence of dendrites often indicates porosity. The solidification model for the truncated cone predicted less than 1% porosity; however, from the image it was not possible to quantitatively determine the size of the pore from the fracture

surface. A non-uniform surface makes it difficult to determine a ratio of pore diameter to cross sectional area; nonetheless there is evidence of microporosity in all the truncated cone blank specimens examined for fractography. Additionally it was shown that the fatigue crack initiated at points of porosity near the surface on fatigue specimens. Although there is evidence of porosity, the size and amount cannot be determined from the fracture surface. Further analysis is undertaken in the microscopy section.

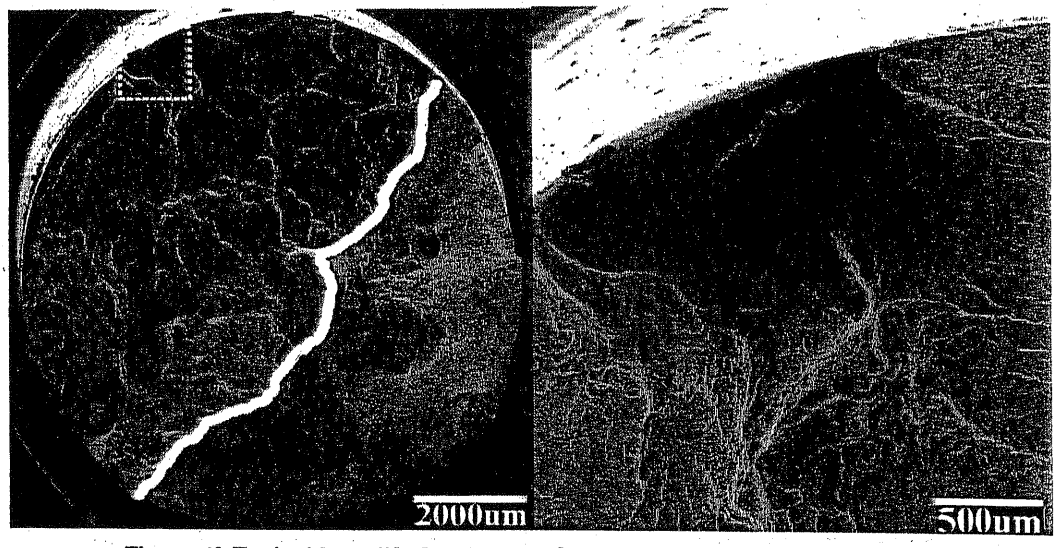

Figure 12 Typical long life fracture surface of a truncated cone specimen

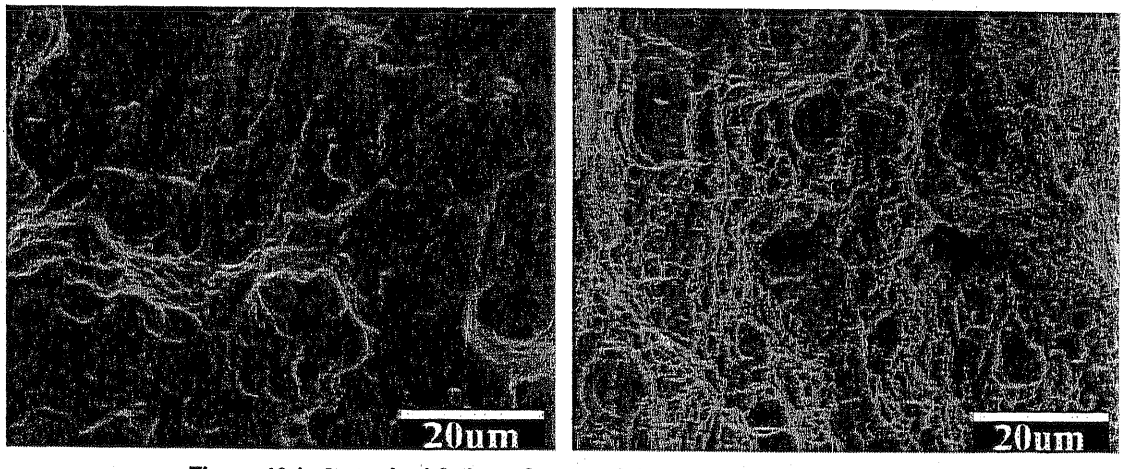

Figure 13 Left: typical fatigue facets; right: typical Ductile Dimpling

STRAIGHT CYLINDER SPECIMEN FRACTOGRAPHY RESULTS

The straight cylinder specimens showed the two types of fatigue fracture seen in the truncated cone specimens; a ductile type fracture and a typical fatigue type fracture. The ductile fracture specimens had fatigue lives of less than 10 000 cycles, while specimens that had more than 10 000 cycles had typical fatigue fractures. Under higher magnification, areas of ductile dimpling were found indicating ductile final fracture in both types of fractures. Fatigue facets in the straight cylinder specimens were also found in the FCG regions. Figure 14 shows a longer life straight cylinder specimen with the two distinct regions divided by a white line, with the FCG region above the white line and the final fracture region with the shear lip below. The longer life specimens showed the same characteristics previously described with the truncated cone specimens. The difference was these fracture surfaces contained extensive dendrite formation seen in the close up fractograph of Figure 14 indicated by the dashed line box. More developed porosity was seen when compared to the truncated cone specimens, and the pores in these specimens also had more texture and extended deeper into the specimen.

FRACTOGRAPHY COMPARISON

The fracture surfaces examined in the Sigl study had similar traits to the current study, except less ductile dimpling was observed. Figure 15 shows a long life specimen from the microporous group. Like the truncated cone specimens there is

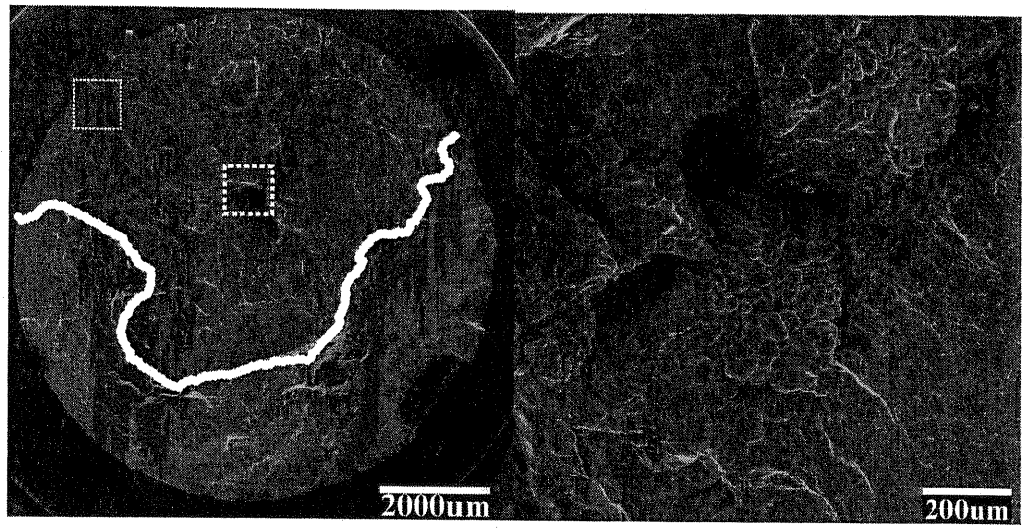

Figure 14 Typical long life fracture surface of a straight cylinder specimen

evidence of porosity, especially at the crack nucleation region, however, macroscopically the specimens appear relatively sound. A clear distinction is also observed between the FCG and the final fracture regions. The amount of porosity in the macroporous specimens from the Sigl study varied greatly, but Figure 16 shows a typical fracture surface. The surface is dominated by dendrite formation, thus the FCG and final fracture regions are not as defined. The straight cylinder specimens from the current study may show deep formation of porosity, but the effects are generally localized to the center. The macroporous specimens tested by Sigl show the porosity developed across the entire cross section, indicating a higher percentage of porosity than seen in the cylindrical specimens.

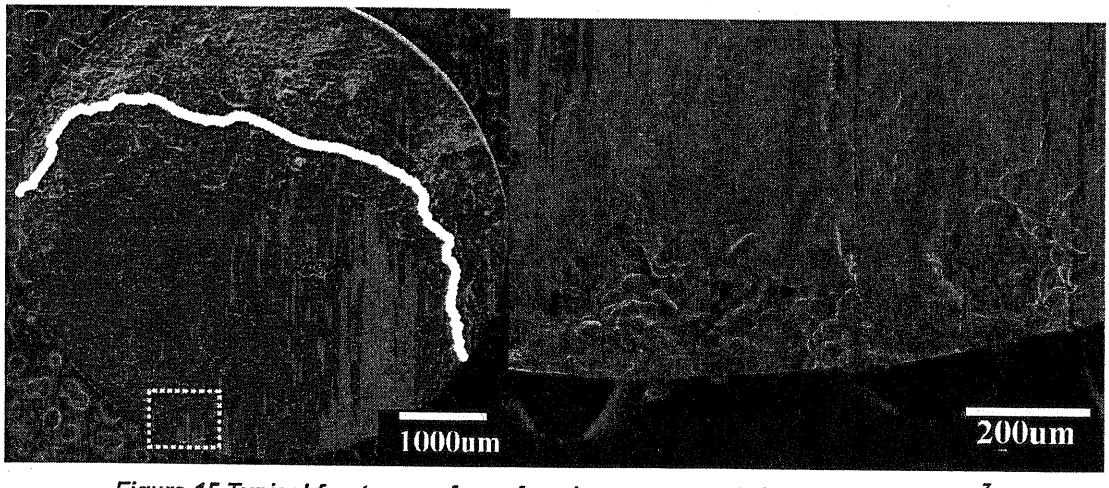

Figure 15 Typical fracture surface of a microporous specimen from Sigl et al.[7]

MICROSCOPY

MICROSCOPY PROCEDURE

In order to quantify the porosity that contributed to fatigue and fracture, a method using fine grinding was employed to remove the fracture surface on the specimens, and then examining this surface using the SEM. Representative specimens were chosen from the two casting geometries. Since porosity was seen on the fracture surfaces, it was desirable to estimate the amount of porosity in a near uniform cross section. Preparation of the specimens was accomplished according to ASTM E03[11]. To investigate the surface for porosity, the SEM was set to 600-1000x and the surface was scanned slowly. For macroporosity, the microscope was centered above spots of interest and pictures were taken at increasing magnification of

20-5000x. For microporosity only clusters of pores could be seen effectively at the scanning rate. Once a cluster was found the magnification was increased to 1500-5000x to examine the porosity.

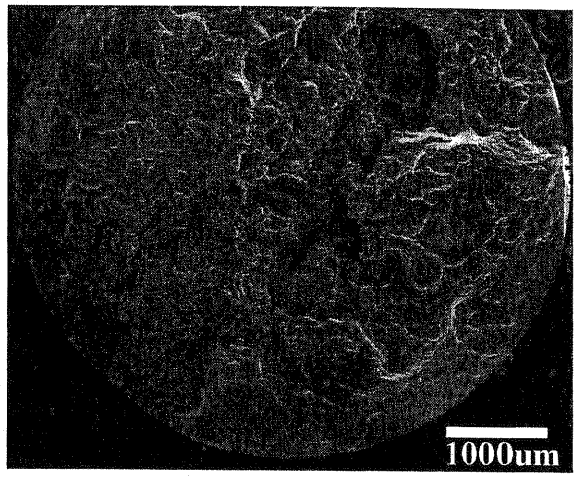

Figure 16 Typical fracture surface of a macroporous specimen from Sigl et al.[7]

TRUNCATED CONE SPECIMEN MICROSCOPY

Radiographic analysis for all the truncated cone specimens indicated no macroporosity, however, all the fracture surfaces viewed showed some evidence of dendrite formation. The macroscopic view of the ground fracture surface from the truncated cone specimens showed no evidence of macroporosity. Scratches were visible along the surface but there was no evidence of macroporosity. The casting simulation indicated no areas of concentrated porosity and therefore, examination for porosity was conducted over different representative areas. At a magnification of 250x it was possible to detect microporosity. Two images are shown in Figure 17 of the typical microporosity found. In this figure the largest pore was measured to have a diameter of just less than 5 microns. This is representative of most of the micropores in the truncated cone specimens. At some locations there was almost no microporosity evident, while at other locations larger micropores were found, but not with the same frequency, and not exceeding 10 microns. Some amount of microporosity is assumed to occur in static casting and cannot be avoided, evidence of this is found in these specimens. This indicates that these specimens were sound.

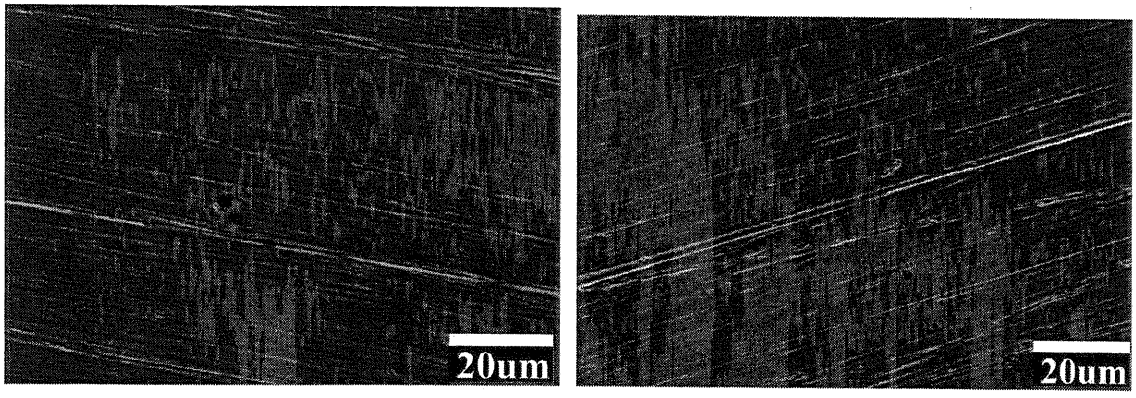

Figure 17 Typical microporosity found in truncated cone specimens

STRAIGHT CYLINDER SPECIMEN MICROSCOPY

The ground fracture surfaces and radiographs of the straight cylinder blank specimens did have evidence of macroporosity. Radiographically there was macroporosity, and in the fractography the straight cylinder specimens showed extensive dendrite formation. A macroscopic view of this specimen does not contain concentrated amounts of macroporosity, but does show multiple sites of small but visible macroporosity. Two of the larger pore sites from the macroscopic images are shown in Figure 18. The largest dimension of the pores were sometimes more than 200 microns as seen in both images, but the majority were on average 100 microns or less as shown at the far left. This porosity may be indicated on the radiograph, but the majority of the pores seem to have a diameter that may not be resolvable by the x-rays due to the section thickness. Inspection of the ground surfaces also revealed microporosity clusters, where most of the pores seen were on the order of at

least 5 microns but at a high density. If these clusters are dense enough through a volume, the radiograph may detect the porosity as a field. These porosity fields do not form simple spheres, however, the voids may be distributed throughout the section, which reduces the density of the material. In these cases a cross-section view may not give the most accurate representation of the extent of which the volume is permeated with voids.

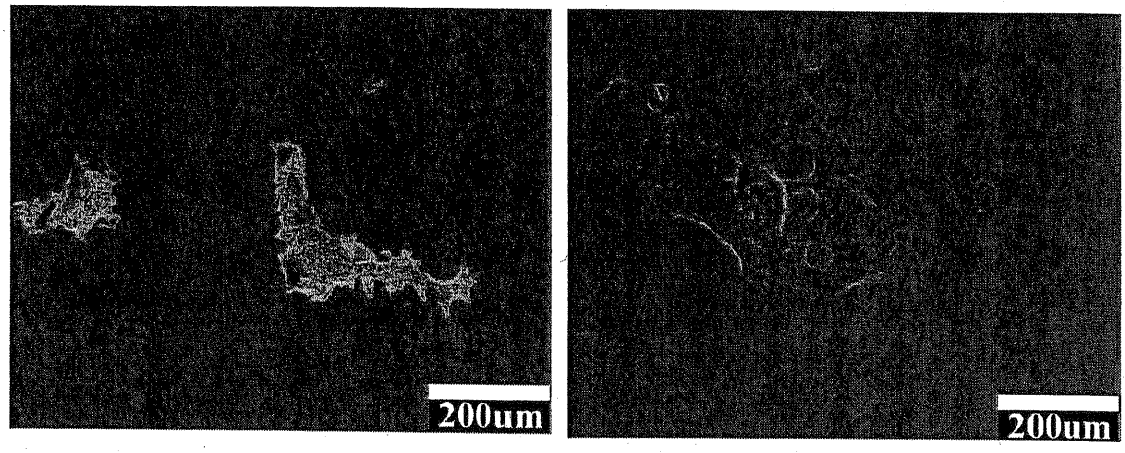

Figure 18 Typical macro and microporosity found in straight cylinder specimens

COMPARISON OF MICROSCOPY

The theoretical limit of resolution for the current research radiographs was ~200 microns. Any porosity that could not be resolved by x-ray was considered microporosity. The truncated cone specimens showed no macroporosity in the radiograph, but there was evidence of possible porosity in the fractography due to the formation of dendrites. In the previous research done by Sigl in 2003[7], testing material showed evidence of microporosity after the fracture surface was ground away. Although the radiographs did not indicate any macroporosity, the typical occurrence of microporosity is shown in the left image of Figure 19 for the Sigl microporous specimens. The surfaces have a distribution of pores that average about 10 microns in diameter. The porosity found in the Sigl microporous specimens is more than the microporosity found in the truncated cone specimens where the microporosity evidence was considered to be incidental from static casting. The ground surfaces of the truncated cone specimens showed pores with a 5 micron diameter average, with a frequency much less than what Sigl found in the previous study for the sound material. This increase of microporosity resulted in the decrease of fatigue life when compared to sound material as shown in the experimental results.

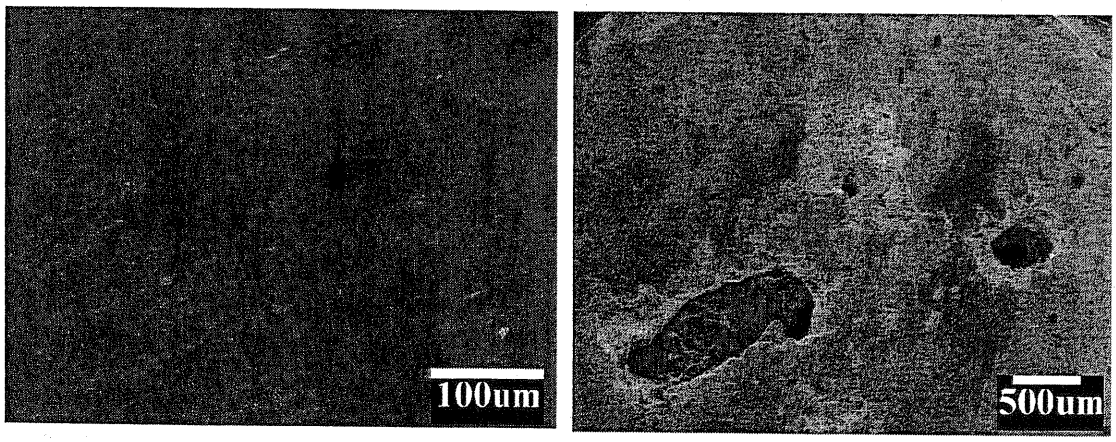

Figure 19 Sigl's microscopy[7], left: microporous specimen, right: macroporous specimen

The right image of Figure 19 shows an example of the ground fracture surface of a Sigl macroporous specimen. These specimens showed a clear indication of macroporosity in the radiographs. The ground surface shows large voids that extend much deeper into the specimen than seen in the straight cylinder specimens of the current research. The straight cylinder specimens showed clear evidence of macroporosity in the radiographs, but the ground surface revealed only small amounts of macroporosity. There was evidence of microporosity too, with diameters reaching ~20 microns at higher densities. The amount of macroporosity shown in the radiograph was not seen in the ground cross sections, rather it is theorized that the density of pores was large enough to show evidence of macroporosity in the radiograph without having contiguous pores that would be visible macroscopically.

DISCUSSION

COMPARISON OF MONOTONIC PROPERTIES

The monotonic results of the truncated cone specimens were supposed to closely resemble the results of the keel block specimens tested for the SFSA[6] in 1983. A keel block is regarded as the most reliable method for obtaining sections of sound material in a casting. The Sigl study used specimens machined from castings that resembled an oversized specimen. The Sigl specimens, however, were found to have significant microporosity that affected some monotonic and fatigue properties[7]. The truncated cones were designed to have a strong temperature gradient that was supposed to minimize the formation of macro and microporosity. Cast steels, regardless, will often contain some porosity.

The ultimate tensile strength, S_u, and modulus of elasticity, E, are similar between the three groups, but Sigl has shown that these values can be close even in the presence of microporosity[7]. The yield strength, S_y, is 14% higher on the truncated cone specimens than the value found for the SFSA study, but only 3% different from the Sigl specimens. The higher S_y with a similar S_u could indicate less ductility, and Sigl found that a lack of ductility can be a sign of microporosity. Percent reduction of area, %RA, is an indicator of the ductility of a material, where Sigl saw only ¼ of the %RA measured in the SFSA study, while the truncated cone specimens saw on average ½ of the SFSA value. The differences between S_y and %RA for the truncated cone specimens in comparison to the SFSA properties may be an indicator of microporosity, but may instead be slight differences in heat treatment, chemistry, or testing procedure. Heat treatment between the three groups was supposed to be identical, yet there was some small variance. The chemistry for the three steels all were within specifications for 8630 cast steel.

S-N COMPARISON OF STRAIGHT CYLINDER AND TRUNCATED CONE SPECIMENS

Using the regression curve from the truncated cone specimens the data from the straight cylinder specimens were superimposed on the plot shown in Figure 9. The lives for the straight cylinder specimens were significantly less than the sound curve as shown by the open triangles and the dashed regression line in Figure 9. Generally their lives were close to an order of magnitude less, and the run-out criterion of $2x10^6$ cycles was not achieved at the run-out stress amplitude level of the truncated cones, ~200 MPa. Two lower stress amplitudes were tested before run-out was achieved. The behavior of the straight cylinder specimens has a similar behavior to the microporous specimens that were tested by Sigl. However, in the radiographs there was evidence of macroporosity, which was not present in the Sigl study microporous specimens. The fractography of the straight cylinder specimens showed more extensive dendrite formation than found in the truncated cone specimens. This shows that the volume of the pores was probably larger than in any of the other specimens. Grinding back the fracture surface did not uncover as much macroporosity as anticipated. There were signs that the porosity was not localized to the center of the specimen, rather it was distributed throughout the specimen test section. The microporosity was also larger and more frequent. The total amount of porosity seen in the ground back fracture surface of the straight cylinder specimens is qualitatively less than 2% and the fatigue lives for the straight cylinder specimens fall consistently less than any of the other specimens except for the Sigl macroporous specimens. This is probably due to the more consistent distribution of porosity throughout the test section. The simulations showed that the center of the straight cylinder casting blank had a higher amount of porosity than the truncated cone, and was spread throughout the length of the casting. Radiographs showed macroporosity in the entire specimen test section lengths for the straight cylinder specimens. This is also consistent with the results of Sigl's testing, showing that microporosity can affect the fatigue life without consuming a large percentage of volume.

COMPARISON OF CYCLIC/FATIGUE PROPERTIES FOR THE THREE STUDIES

Using the cyclic and fatigue properties, the three studies can be compared to further determine their similarities and differences. The cyclic stress-strain curve for the truncated cone specimens showed some inconsistent trends. The peak stress values were lower for some of the higher strain amplitude specimens. This is shown in the hysteresis loops in Figure 6. This was most likely due to the inability of the specimens to reach a steady stress amplitude during strain controlled fatigue testing. Figure 5 demonstrated how higher strain amplitude specimens continued to have falling stresses over their lives. Initially there is evidence of cycle softening, but the stress never obtained a steady value for any portion of the life. The lower strain amplitude specimens from 0.005-0.0035 exhibit somewhat more consistent behavior, but cycle hardened initially instead. These results prompted the use of an incremental fatigue test specimen. Although the specimen did not have the higher strain amplitudes of 0.01 and 0.008, it still exhibited the same trends seen in the companion method. The highest strain amplitude 0.006 had a lower peak stress than the next lowest amplitude. This is demonstrated in the hysteresis loops for the incremental specimen, which are shown in Figure 7.

Comparing the cyclic and fatigue properties for the truncated cone specimens to Sigl's and the SFSA results show some similarities and differences. The fatigue strength, S_f at $2x10^6$ cycles, for the truncated cone specimens is 28% higher than the value found by Sigl, but is still 29% lower than the benchmark value of the SFSA specimens. The fatigue strength can be dependent on the ability to resist crack initiation. The truncated cone specimens were designed with larger dimensions than

the previous two studies, so if the amount of microporosity was consistent with the keel block specimens there would have been a greater ability to develop fatigue cracks due to the increased surface area of the larger specimen. Sigl's microporous specimens had a lower S_f due to microporosity; the pores acted as a local stress riser and initiated fatigue crack growth. The cyclic strength coefficient, K', and cyclic strain hardening exponent, n', for the truncated cone specimens were closer to the values found for the keel block specimens than for Sigl's microporous specimens. Using Equation (8) these values can be used to calculate a representative cyclic stress-strain curve for each study.

$$\varepsilon_a = \frac{\sigma_a}{E} + \left(\frac{\sigma_a}{K'}\right)^{1/n'} \qquad \text{Equation 8}$$

Comparison of the cyclic stress-strain behavior of the different studies showed that the SFSA specimens tended to cycle soften more rapidly than the other two studies. The cyclic yield strength, S_y', is dependent on this behavior, and was higher for both the truncated cone specimens and Sigl's specimens by more than 25%, when compared to the averaged benchmark value for the sound material from the SFSA study. This is consistent with the increased S_y found for the monotonic values. The cyclic behavior is not conclusive of the relative soundness of the material. Cyclic softening and hardening is controlled by the microstructure of the material. Although micropores can have considerable impact, the amount of micropores seen in the microscopy was minimal. Furthermore the size of the micropores is small enough that the stress concentration in fatigue should have negligible effects on the life. Grain size and crystalline structure is more influential for cyclic behavior, and is dependent on factors such as heat treatment and chemistry.

Using a strain-life comparison the fatigue behaviors can be compared. The fatigue ductility exponent, c, and the fatigue ductility coefficient, ε_f', are indicators of the amount of plastic strain the material exhibits during cycling. Likewise the fatigue strength exponent, b, and the fatigue strength coefficient, σ_f', are indicators of the elastic strain exhibited. These values can be used to plot curves that represent the strain-life behavior of the material. The intersection of these curves is the transition fatigue life and indicates when the deformation is mainly elastic or plastic. The keel block has an early intersection of the plastic and elastic strain curves, while the truncated cone specimens and Sigl's microporous specimens elastic and plastic strain curves never intersect. This indicates that specimens in this current study and Sigl's specimens are dominated by elastic deformation, and have less plasticity. This is consistent with the lower ductility and high S_y'. The combination of these lines represents the complete strain-life behavior of the material. From Figure 10 the S-N curve is shown for the specimens from the Sigl study. The microporous specimens follow a similar behavior trend as the current study and the SFSA study, however, the macroporous specimens only roughly fit the trend. The macroporous specimen data show only a slightly decreasing trend of stress to fatigue life, but with a significant reduction in fatigue resistance. In addition, Young's modulus, E, as shown in Table 3 is significantly lowered for the macroporous specimens.

Figure 11 shows a comparison of the current research (truncated cone and straight cylinder specimens), the SFSA keel block specimens, and Sigl's research (microporous and macroporous specimens). The Sigl microporous specimens clearly have less fatigue resistance than the keel block and truncated cone specimens, but better fatigue resistance than the straight cylinder specimens. The truncated cone and keel block specimens have similar behavior up to ~15 000 cycles; then the two curves deviate which is primarily dependent on elastic behavior. This effect may again be attributed to the heat treatment, chemistry, testing accuracy, or the size difference. It can be concluded from the S-N curves, that the truncated cone specimens come much closer to representing sound material than the specimens Sigl tested.

Further evidence to show that the truncated cone specimens were sound was through the use of fractography and microscopy. The fractography for the truncated cone specimens revealed dendrite formation in the fracture surface, which may have been a sign of porosity. However, the amount and size could not be measured since the cross sectional area was too irregular. The microscopy procedure was developed to show a representative amount of porosity that caused fracture. After grinding the fracture surface back, a two-dimensional representation of the porosity was revealed near the fracture zone. The porosity that was found was all microscopic which is validated by the radiographs. The average size of a pore was found to be ~5 microns with very few present. Sigl saw pores at a slightly larger size with many more present. Qualitatively the amount of microporosity found in Sigl's research was much higher than seen in the truncated cone specimens. The microporosity seen in the truncated cone specimens was concluded as being incidental porosity that occurs naturally in casting, and the truncated cone specimen can be considered basically sound material.

SUMMARY AND CONCLUSIONS

The fatigue resistance of five 8630 cast steel specimen groups that involved essentially the same heat treatment and chemistry were compared based on porosity present. The porosity of the five specimen groups ranged from sound (keel block and truncated cone), to microporous (Sigl microporous), to microporous and macroporous (straight cylinders), and to macroporous (Sigl macroporous).

1. Monotonic and cyclic tests for keel block, truncated cone and Sigl's microporous specimens[7] resulted in cyclic softening, similar values of S_u and E, but lower S_y and S_y' and higher %RA for keel block specimens.
2. Strain-controlled LCF truncated cone specimen tests indicated non-steady state hysteresis loops during cycling that provided difficulty in obtaining the cyclic stress-strain response.
3. Fatigue resistance of the five groups of porosity was directly related to the type and quantity of porosity. The sound keel block specimens had the greatest fatigue resistance followed by the sound truncated cone specimens, Sigl microporous specimens, straight cylinder micro/macroporous specimens, and then the Sigl macroporous specimens.
4. Fatigue limits, S_f, at 2 to $5x10^6$ cycles ranged from 293 MPa for the keel block specimens to less than 40 MPa for the Sigl macroporous specimens. This is about a 6:1 range which is very significant. However, excluding the Sigl macroporous specimens with their extremely large porosity, S_f ranged from 293 to 126 MPa or a 2.3:1 range which is much more reasonable for functional steel castings. In the finite life region, and neglecting the Sigl macroporous data, fatigue lives varied from one to two orders of magnitude.
5. Fatigue fracture surfaces for the truncated cone and straight cylinder specimens in the LCF region resembled tensile fractures, whereas in the HCF region both fatigue crack growth and final fracture regions were evident. SEM fractography revealed fatigue facets in the FCG region and ductile dimples in the final fracture region. Extensive dendrite formation existed in the fracture surfaces of the straight cylinder specimens indicating macroporosity.
6. SEM microscopy revealed only a few incidental widely spaced small micropores (about 5 μm) in the truncated cone specimens adding to the conclusion of their soundness. Both micro and macroporosity were found in the straight cylinder specimens with most macropore sizes around 100 μm in diameter.

ACKNOWLEDGMENTS

This research was funded by the United States Department of Defense through the American Metalcasting Consortium (AMC) PRO-ACT program. AMC's PRO-ACT program is sponsored by the Defense Supply Center Philadelphia, Philadelphia, PA the Defense Logistics Agency, Ft. Belvoir, VA, and the Army Research Laboratory. This research was conducted under the auspices of the Steel Founders' Society of America, and through substantial in-kind support from SFSA member foundries. In particular, we would like to thank Alloy Weld Inspection Co. for their digital and film radiography of the fatigue test specimens, Southern Cast Products for building the test specimen casting pattern and casting test specimens, and MAGMA GmbH for their support of the porosity prediction model used to design the test specimen castings. Any opinions, findings, conclusions, or recommendations expressed herein are those of the authors and do not necessarily reflect the views of DSC, DLA, or the SFSA and any of its member foundries.

REFERENCES

1. Wang, Q. G., Apelian, D., Lados, D. A., "Fatigue Behavior of A356-T6 Aluminum Cast Alloys. Part I. Effect of Casting Defects." *Journal of Light Metals*, Vol. 1, 2001, pp. 73-84.
2. Buffiere, J. Y., Savelli, S., Jouneau, P. H., Maire, E., Fougeres, R., "Experimental Study of Porosity and its Relation to Fatigue Mechanisms of Model A.-Si7-Mg0.3 Cast Al Alloys." *Materials Science and Engineering A*, Vol. 316, 2001, pp. 115-126.
3. Maino, R., Wallace, J. F., "Fatigue Behavior of Various Grades of Steel Castings and the Influence of Cast Surfaces." Institution of Mechanical Engineers, Conference Publications, 1979, pp. 439-476.
4. Kohno, M., Makioka, M., "Some Studies on the Manufacture of Cast 13 Chrome Stainless Steel Francis Type Runners for Hydraulic Turbines," *AFS Transactions*, 1970, pp. 9-16.
5. Chijiwa, K., Nakayama, T., Imamura, M., "Effect of Casting Defects upon the Endurance Limit of Large Steel Castings." 35e CIF, Vol. 36, pp. 1-12.
6. Stephens, R.I., *Fatigue and Fracture Toughness of Five Carbon or Low Alloy Cast Steels at Room or Low Climatic Temperatures*. Research Report No. 94A, Carbon and Low Alloy Technical Research Committee, Steel Founders' Society of America, Des Plaines, IL, 1982.
7. Sigl, K. M., Hardin, R. A., Stephens, R. I., Beckermann, C., "Fatigue of 8630 Cast Steel in the Presence of Porosity", *International Journal of Cast Metals Research*, Vol. 17, No. 3, 2004, pp. 130-146.
8. Standard E18. "Verifications of Machines for Rockwell Hardness and Rockwell Superficial Hardness Testing" *2004 Annual Book of ASTM Standards*, Vol. 03.01, American Society of Testing and Materials, West Conshohocken, PA, 2004, pp. 138-149.
9. Steel Founders' Society of America, *Steel Castings Handbook*, 6th ed., Steel Founders' Society of America, Materials Park, OH, 1995.
10. Standard E606. "Standard Practice for Strain-Controlled Testing" *2004 Annual Book of ASTM Standards*, Vol. 03.01, American Society of Testing and Materials, West Conshohocken, PA, 2004, pp. 592-606.
11. Standard E3. "Standard Guide for Preparation of Metallographic Specimens." *2004 Annual Book of ASTM Standards*, Vol. 03.01, American Society of Testing and Materials, West Conshohocken, PA, 2004, pp. 1-12.